

# Nanoscale anglesite growth on the celestite (001) face

Carlos M. Pina\* and Aida Rico-García

Department of Crystallography and Mineralogy, Complutense University of Madrid, 28040

Madrid, Spain

## ABSTRACT

In situ atomic force microscopy (AFM) was used to study the growth behaviour of anglesite ( $\text{PbSO}_4$ ) monolayers on the celestite (001) face. Growth was promoted by exposing the celestite cleavage surfaces to aqueous solutions that were supersaturated with respect to anglesite. The solution supersaturation,  $\beta_{ang}$ , was varied from 1.05 to 3.09 (where  $\beta_{ang} = a(\text{Pb}^{2+}) \cdot a(\text{SO}_4^{2-}) / K_{sp,ang}$ ). In this range of supersaturation, two single anglesite monolayers ( $\sim 3.5$  Å in height each) from pre-existent celestite steps were grown. However, for solution supersaturation of the values of  $\beta_{ang} < 1.89 \pm 0.06$ , subsequent multilayer growth is strongly inhibited. AFM observations indicate that the inhibition of a continuous layer-by-layer growth of anglesite on the celestite (001) face is due to the in-plane strain generated by the slight difference between the anglesite and celestite lattice parameters (i.e. the linear misfits are lower than 1.1%). The minimum supersaturation required to overcome the energy barrier for multilayer growth gave an estimate of the in-plane strain energy:  $11.4 \pm 0.6$  mJ/m<sup>2</sup>. Once this energy barrier is overcome, a multilayer Frank–van der Merwe epitaxial growth was observed.

Keywords: Surface topography; Atomic force microscopy; Crystal Growth; Epitaxy; Aqueous solutions; Solid–liquid interfaces; Celestite; Anglesite

---

\* Author to whom correspondence should be addressed (cmpina@geo.ucm.es)

## 1. Introduction

Epitaxial growth has been intensively studied during the last century, due to its importance for both crystal growth theories and the development of technological devices [1,2]. Moreover, it has recently been shown that epitaxial growth on mineral surfaces can play an important role in the removal of heavy metals from polluted aqueous environments [3,4]. The development of both oriented overgrowths with suitable technological properties and the ability of mineral surfaces to clean contaminated waters strongly depend on the characteristics and kinetics of the epitaxial growth. Pioneering works by Frank and van der Merwe [5], Volmer and Weber [6] and Stranski and Krastanov [7] proposed three general models to describe the main epitaxial modes observed in nature and in the laboratory [1]. In all of these models, the growth behaviour of the epitaxial layers is explained in terms of the substrate-overgrowth adhesion forces. Such adhesion forces are mainly determined by bond strengths, lattice misfits and their related strain energies. Therefore, the study of the formation of the first monolayers on a given substrate is essential for testing the proposed models and providing qualitative and quantitative information about the factors controlling epitaxial growth kinetics.

Atomic force microscopy (AFM) is a powerful tool for investigating crystal growth at a nanoscale. In particular, AFM can examine the epitaxial growth from aqueous solutions [8-12]. Using AFM, it is possible to directly observe the formation of the very first epitaxial monolayers that grow over crystalline substrates; these monolayers are only a few angstroms in thickness. In addition, *in situ* AFM experiments allow us to determine overgrowth-substrate crystallographic relationships and quantify the kinetics of successive monolayers as a function of supersaturation. The information provided by AFM experiments in the literature confirms that there are three main epitaxial growth mechanisms [11-13]. However, detailed investigations have also revealed that the

growth kinetics of monolayers are not directly predicted by the classical growth models. In this respect, a number of AFM measurements on both heteroepitaxial and homoepitaxial systems have shown that the first monolayers frequently have a singular growth behaviour that leads to a partial or total inhibition of further layer-by-layer continuous growth [14, 15 and references therein]. As a result, a reproduction of the original nanotopographic features (i.e. the so-called template effect) can occur [15-17]. Although this phenomenon seems to be related to the generation of strained areas on the first monolayers, a conclusive explanation has not been reported.

In this paper, we present *in situ* AFM observations of the epitaxial growth of the first monolayers of anglesite ( $\text{PbSO}_4$ ) on the celestite (001) face. The anglesite-celestite epitaxial system is a suitable model for studying the kinetics of the Frank-van der Merwe layer-by-layer growth mechanism. By measuring the dependence of the velocities of the  $\text{PbSO}_4$  monolayers on the supersaturation we evaluated the effect of surface strain on the kinetics of continuous multilayer growth. The aim of this paper is to provide a better understanding of the factors that determine the frequent singular behaviour of the first monolayers in epitaxial systems.

## 2. Experimental Procedure

*In situ* growth experiments on the celestite (001) face were performed at room temperature in the fluid cell of a Digital Instruments Multimode AFM. The celestite ( $\text{SrSO}_4$ ) samples were optically clear single crystals. These crystals were freshly cleaved along the (001) face prior to each growth experiment and placed in the fluid cell of the AFM. At the start of each experiment, deionised water (milliQ; 18  $\text{M}\Omega\cdot\text{m}$ ) was passed over the celestite (001) surface. Anglesite growth was promoted by passing aqueous solutions with increasing supersaturations (with respect to anglesite) over the substrate. The solutions were prepared

**Table 1.**

Concentrations, activities and supersaturations with respect to anglesite of the solutions used in the AFM experiments.

Experiment number	Solution composition				Supersaturation
	PbCl <sub>2</sub> (mmol/l)	Na <sub>2</sub> SO <sub>4</sub> (mmol/l)	$a(Pb^{2+})$	$a(SO_4^{2-})$	$\beta_{ang}$
1	0.16	0.16	$1.29 \times 10^{-4}$	$1.31 \times 10^{-4}$	1.05
2	0.18	0.18	$1.43 \times 10^{-4}$	$1.46 \times 10^{-4}$	1.29
3	0.20	0.20	$1.57 \times 10^{-4}$	$1.60 \times 10^{-4}$	1.55
4	0.21	0.21	$1.64 \times 10^{-4}$	$1.67 \times 10^{-4}$	1.70
5	0.22	0.22	$1.70 \times 10^{-4}$	$1.73 \times 10^{-4}$	1.82
6	0.23	0.23	$1.77 \times 10^{-4}$	$1.80 \times 10^{-4}$	1.95
7	0.24	0.24	$1.83 \times 10^{-4}$	$1.87 \times 10^{-4}$	2.11
8	0.25	0.25	$1.90 \times 10^{-4}$	$1.94 \times 10^{-4}$	2.29
9	0.26	0.26	$1.96 \times 10^{-4}$	$2.00 \times 10^{-4}$	2.40
10	0.27	0.27	$2.02 \times 10^{-4}$	$2.07 \times 10^{-4}$	2.57
11	0.28	0.28	$2.09 \times 10^{-4}$	$2.14 \times 10^{-4}$	2.75
12	0.30	0.30	$2.21 \times 10^{-4}$	$2.26 \times 10^{-4}$	3.09

using high-purity Na<sub>2</sub>SO<sub>4</sub> and PbCl<sub>2</sub> solutions and deionised water. The expression used to calculate the supersaturation with respect to anglesite is:  $\beta_{ang} = a(Pb^{2+}) \cdot a(SO_4^{2-}) / K_{sp,ang}$ , where  $K_{sp,ang} = 10^{-7.886}$  is the solubility product for anglesite and  $a(Pb^{2+}) \cdot a(SO_4^{2-})$  are the activities of the Pb<sup>2+</sup> and SO<sub>4</sub><sup>2-</sup> ions in the aqueous solution. The activities of Pb<sup>2+</sup> and SO<sub>4</sub><sup>2-</sup> were calculated using the PHREEQC computer code [18]. The composition of the solutions, ionic activities and supersaturations with respect to anglesite are listed in Table 1. In order to maintain constant supersaturation in the fluid cell, more solution was injected in intervals of about 1 min in between each AFM scan. All of the images presented in this work were taken in constant force mode while displaying the cantilever deflection signal. Height images were also captured in order to measure the thickness of the anglesite monolayers. From sequences of deflection images, the monolayer growth rates were measured along the celestite <120> directions.

### 3. Results

Prior to injecting a PbSO<sub>4</sub> aqueous solution into the fluid cell of the AFM, deionised water was passed over the celestite (001) surfaces. This resulted in both the slight dissolution of cleavage steps and the nucleation and growth

of typical triangular-shaped etch pits with a depth of half of a unit cell ( $\sim 3.4$  Å) [19]. The formation of the etch pits allowed us to determine the crystallographic directions of the celestite (001) face (see Fig.1a). Then, solutions that were supersaturated with respect to anglesite were passed over the slightly dissolved celestite (001) faces. Even for low supersaturations, we observed growth from pre-existent cleavage steps and the filling of triangular-shaped etch pits. The half-unit-cell pits were filled with one monolayer of PbSO<sub>4</sub> (see Fig.1b). Measurements show that the PbSO<sub>4</sub> monolayers that advanced from celestite steps and filled the etch pits are about 3.8 Å in height. After the etch pits were filled, a subsequent PbSO<sub>4</sub> monolayer spread over the celestite surface. On this layer, the distribution and shape of the etch pits underneath was revealed by a contrast in both the height and deflection images (see Fig.1c).

After a continuous monolayer is grown over the entire surface, a new PbSO<sub>4</sub> monolayer can grow. However, the growth of this monolayer was not continuous when solutions with  $\beta_{ang} < 1.95$  were used, i.e. the monolayer spreads over the celestite surface except on the areas over the buried etch pits.

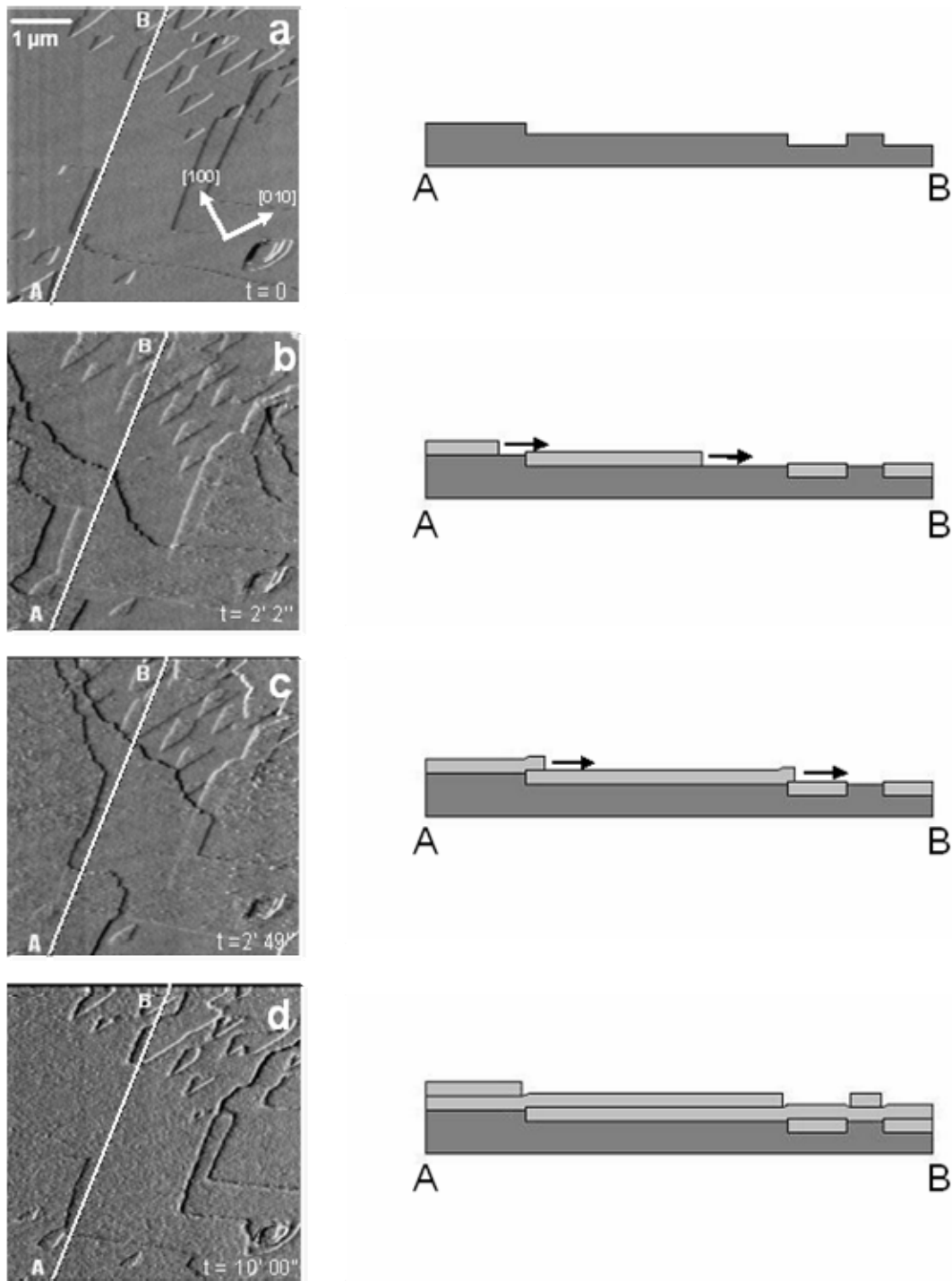


**Fig.1.** Growth sequence of anglesite monolayers on a celestite (001) surface from a solution with  $\beta_{ang} = 1.70$ . (a) Triangular etch pits after dissolution in water. (b) Growth of a first anglesite monolayer, which fills the etch pits. (c) Advancement of a monolayer on the previously formed anglesite first monolayer. (d) Growth of a subsequent anglesite monolayer that reproduces the original nanotopography (compare image (a) with (d)). Profiles along the A-B lines are drawn on the right side of each image to show the relationship between the celestite substrate and the growing anglesite monolayers. Scale bar and crystallographic directions (white arrows) on image (a) are valid for all the images. Elapsed times from the start of the experiment are shown in the bottom right-hand corner of each AFM image.

The result is an almost perfect reproduction of the original celestite surface (compare Fig.1a with Fig1d). In contrast, for solutions with  $\beta_{ang} > 1.95$ , the  $\text{PbSO}_4$  monolayer was able to cover the entire surface and only a slight contrast in the AFM images reveals the position of the buried etch pits (see Fig 2). Moreover, for solutions with  $\beta_{ang} > 1.95$ , a continuous layer-by-layer growth mechanism was observed. Fig. 3 shows the dependence of the growth rates of successive  $\text{PbSO}_4$  monolayers on supersaturation.

A continuous multilayer growth of  $\text{PbSO}_4$  was also observed at celestite screw dislocations. Fig.4a. shows a group of screw dislocations emerging on a celestite (001) face. This image was taken in water and a slight dissolution of the surface caused the steps generated at the dislocation cores to split into half-steps [9]. While in contact with a solution with  $\beta_{ang} = 2.3$ , the steps grew but the development of spiral hillocks did not occur

for observation times longer than 1 hour (Fig.4b-c). In contrast, when the supersaturation of the solution was increased ( $\beta_{ang} = 3.1$ ), steps were continuously generated at the dislocation cores and spiral growth was rapid (Fig.4d-f). The first steps were roughly parallel to the celestite  $\langle 120 \rangle$  directions and their edges were jagged. However, as the number of steps increased, the step edges became more rounded and the spiral hillocks became more elongated along the  $[010]$  direction. Spiral hillocks formed by more than about six monolayers have a lens shape that is similar to that of spiral hillocks on pure celestite and barite (001) faces (see Fig.5) [19,9]. For higher solution supersaturations, lens-shaped two-dimensional islands were the predominant step generation mechanism and rapid multilayer growth on the celestite (001) faces was observed.

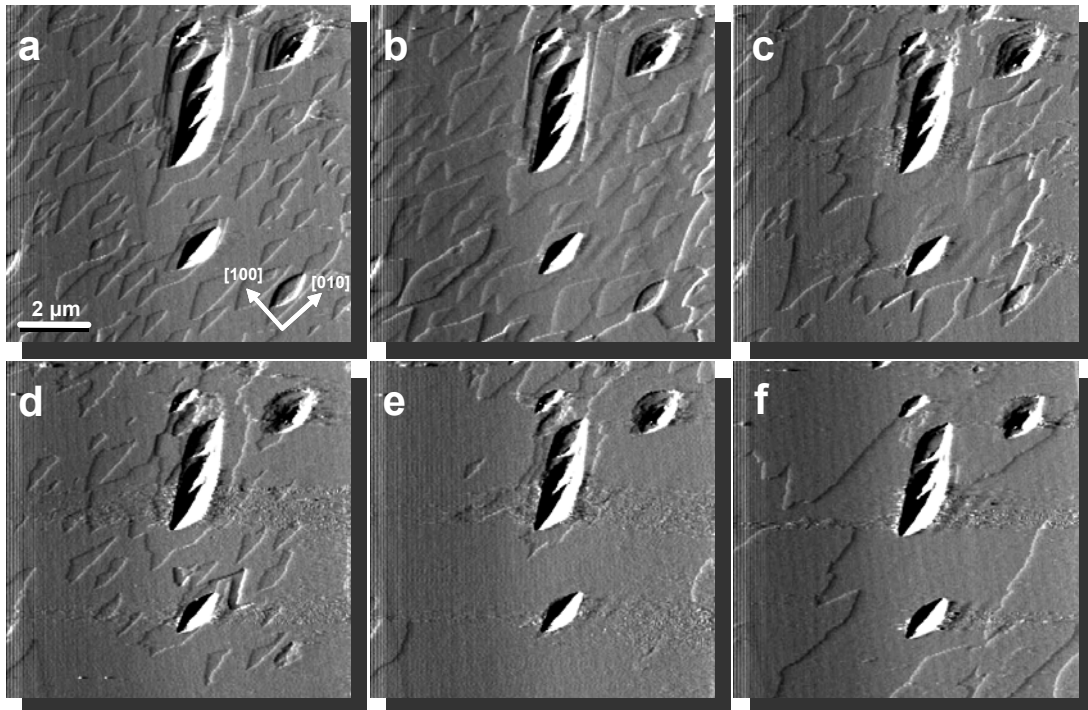


**Fig. 2.** Growth sequence of about 9 minutes, showing the advancement of anglesite monolayers on a celestite (001) surface from a solution with  $\beta_{ang} = 1.95$ . This supersaturation is high enough to promote continuous multilayer growth of anglesite. (a) Celestite (001) surface in water; the triangular etch pits are visible. (b) Etch pits are filled with an anglesite monolayer. (c-f) Growth of successive anglesite monolayers. Scale bar and crystallographic directions (white arrows) on image (a) are valid for all the images.

#### 4. Discussion

The AFM observations presented in the previous section demonstrate that anglesite monolayers can grow in structural continuity with mono-steps on the celestite (001) face. These observations are in agreement with previous reports on the growth of a  $\text{PbSO}_4$  monolayer on two-dimensional  $\text{SrSO}_4$  islands that were pre-grown on a  $\text{BaSO}_4$  substrate [20]. In addition, at supersaturations of  $\beta_{ang} > 1.95$ , the anglesite overgrowth on celestite surfaces occurs by a continuous layer-by-layer mechanism, as predicted by the Frank–van der Merwe epitaxial growth theory [1,5]. According to the Frank–van der Merwe model, the formation of epitaxial monolayers implies a strong adhesion between the substrate and overgrowth. This adhesion is mainly due to the coincidence of similar crystallographic directions and the existence of low linear misfits between these directions. This is consistent with the fact that anglesite and celestite are isostructural minerals with similar lattice parameters: they crystallise in the orthorhombic space group  $Pnma$  with the cell parameters  $a_{ang} = 8.478 \text{ \AA}$ ,  $b_{ang} = 5.397 \text{ \AA}$  and  $c_{ang} = 6.958 \text{ \AA}$  for anglesite, and  $a_{cel} = 8.389 \text{ \AA}$ ,  $b_{cel} = 5.365 \text{ \AA}$  and  $c_{cel} = 6.885 \text{ \AA}$  for celestite [21, 22]. Considering the parallelism between the main anglesite and celestite crystallographic directions, linear misfits can be calculated using the following expression:

$$\delta_{uvw} = \left| \frac{l_{cel}^{uvw} - l_{ang}^{uvw}}{l_{ang}^{uvw}} \times 100 \right| \quad (1)$$

where  $l_{cel}^{uvw}$  and  $l_{ang}^{uvw}$  are the repeating periods along the celestite and anglesite common directions. Using Eq. (1) we obtained the following linear misfits:  $\delta_{100} = 1.05\%$ ;  $\delta_{010} = 0.59\%$ ;  $\delta_{001} = 1.05\%$  and  $\delta_{120} = 0.76\%$ . These misfits are low compared with those calculated for other epitaxial pairs in the same isostructural family: celestite-barite ( $\delta_{100} = 5.51\%$ ;  $\delta_{010} = 1.61\%$ ;  $\delta_{001} = 3.76\%$  and  $\delta_{120} = 3.06\%$ ), anglesite-barite ( $\delta_{100} = 4.83\%$ ;  $\delta_{010} =$

$1.07\%$ ;  $\delta_{001} = 2.89\%$  and  $\delta_{120} = 0.74\%$ ) and hashemite-barite ( $\delta_{100} = 2.56\%$ ;  $\delta_{010} = 1.67\%$ ;  $\delta_{001} = 2.64\%$  and  $\delta_{120} = 2.02\%$ ). For all of these overgrowth-substrate pairs, epitaxial growth mechanisms different than the Frank–van der Merwe mechanism were observed: Volmer-Weber growth was observed for celestite on barite [11] and anglesite on barite [23], and Stranski-Krastanov growth was reported for hashemite on barite [12].

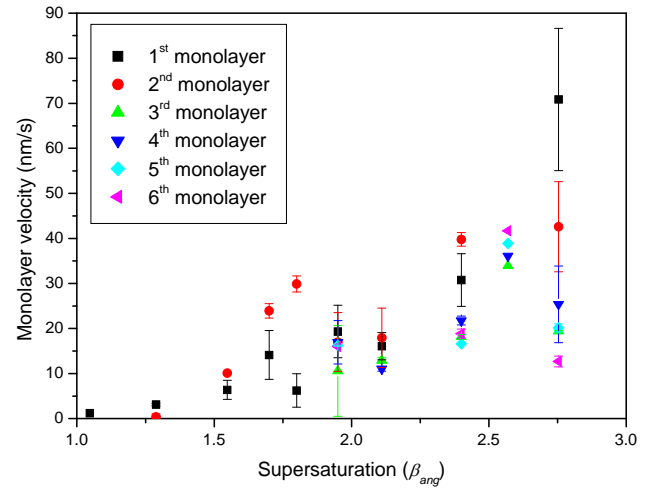


**Fig. 3.** Growth rates of the first six anglesite epitaxial monolayers versus the supersaturation with respect to anglesite.

Although the linear misfits between the anglesite and celestite directions are low, our AFM observations revealed that at low supersaturations ( $\beta_{ang} < 1.95$ ) the multilayer growth of anglesite on the celestite (001) face is strongly inhibited. This inhibition must be related to the lattice strain generated during the growth of anglesite monolayers on the celestite substrate. In order to evaluate the effect of lattice strain on the growth behaviour of anglesite on celestite (001), it is useful to analyse the filling and subsequent burying of etch pits. As described in the previous section, triangular-shaped celestite etch pits with a depth of half of a unit cell can be rapidly filled with a  $\text{PbSO}_4$  monolayer exhibiting an homogeneous strain distribution over large areas (Fig. 1b). This monolayer can experience

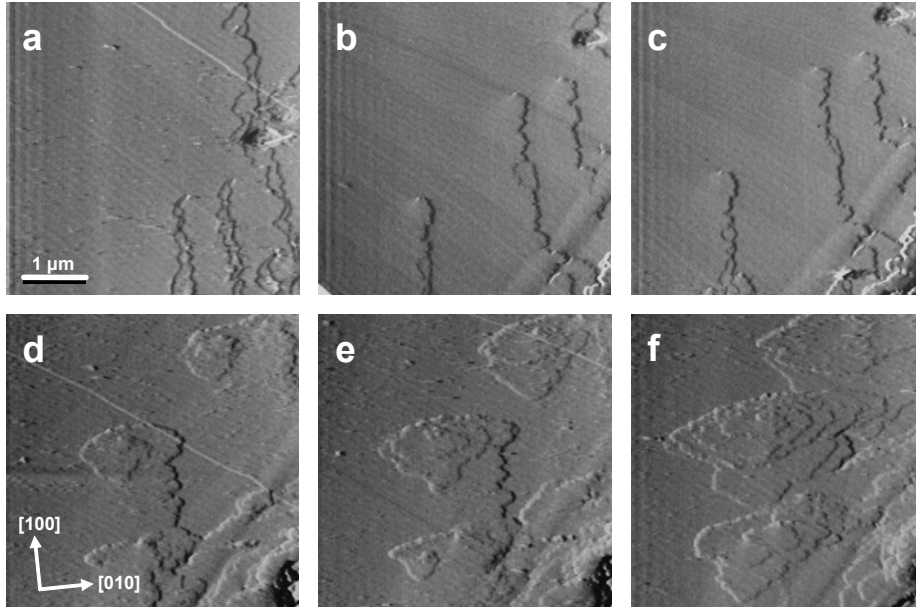


**Fig. 4.** Sequence showing the growth of anglesite monolayers from celestite screw dislocations on a celestite (001) surface. (a) Dissolution of the surface in water causes the separation of the cleavage steps into half-steps. (b–c) Growth from a solution with  $\beta_{ang} = 2.29$ . Although the advancement of anglesite monolayers occurs, no spiral hillocks develop. (d–f) Rapid growth of anglesite spirals from a solution with  $\beta_{ang} = 3.09$ . White arrows on (d) indicate crystallographic directions. The scale bar on image (a) is valid for all the images.

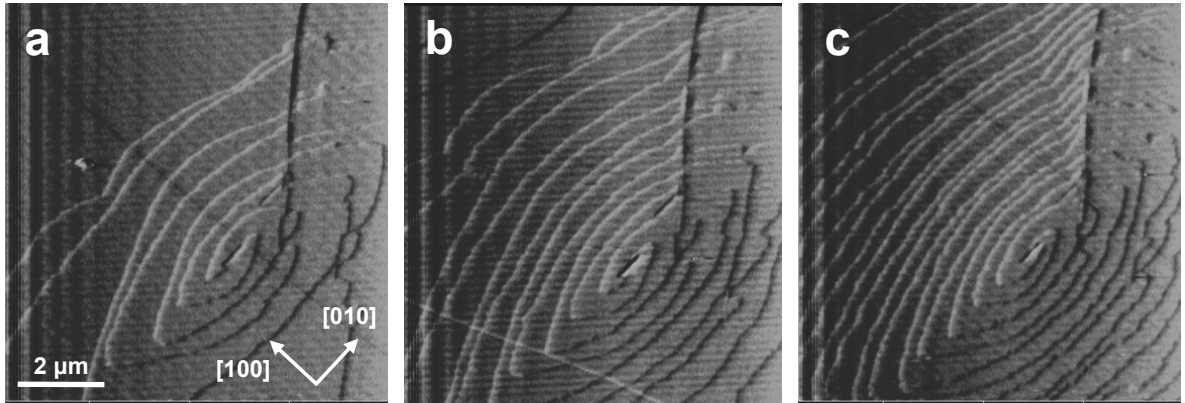


**Fig. 5.** Spiral growth of anglesite on a celestite (001) surface from a solution with  $\beta_{ang} = 2.57$ . The growth velocity of the steps is about 23.2 nm/s. The whole sequence took about 4.5 minutes. scale bar and crystallographic directions (white arrows) on image (a) are valid for all the images.

a significant level of vertical strain, i.e. perpendicular to the celestite (001) face, which is consistent with the measured monolayer height of  $\sim 3.8$  Å, i.e. slightly larger than expected for an unrelaxed monolayer of  $\text{PbSO}_4$  (3.48 Å). Although this difference in height implies the formation of a sub-nano step, it does not preclude the growth of a second monolayer. However, in a second  $\text{PbSO}_4$

monolayer, an inhomogeneous in-plane strain distribution occurs when it grows over the sub-nano step. As a result, the second monolayer is not homogeneously strained at the areas corresponding to the etch pits. Unlike the sub-nano steps, these in-plane strained areas provide a barrier to further monolayer growth. Thus, when a third monolayer reaches the strained area, growth is inhibited and the

shapes of the original celestite etch pits are reproduced. The reproduction of such surface features on a nanoscale after monolayer growth is a common phenomenon observed in a number of experimental systems; it is often referred to as the template effect [14-17]. Although a conclusive explanation has not been reported yet, the template effect is often qualitatively explained by invoking compositional inhomogenities and their related lattice strains [12,14].

In the case of the growth of pure anglesite monolayers on the celestite (001) face, the lattice strain cannot be attributed to compositional inhomogenities. In addition, the template effect vanishes at high supersaturations, indicating that the strain energy barrier can be overcome. Our AFM observations show that for supersaturations higher than  $\beta_{ang}^{min} = 1.89 \pm 0.06$ , a  $\text{PbSO}_4$  monolayer can grow over the strained areas. The minimum supersaturation required for continuous growth can be used to estimate the local strain energy  $\gamma_{strain}$  in the second  $\text{PbSO}_4$  monolayer that is grown over the filled etch pits. To this end, consider the following equilibrium condition for a monolayer growing on a strained substrate from an aqueous solution:

$$-\Delta\mu\left(\frac{A}{a_{st}}\right) + A\gamma_{strain} = 0 \quad (2)$$

where  $\Delta\mu$  is the change in the chemical potential when a growth unit is attached to the monolayer edge from the aqueous solution ( $\Delta\mu = kT \ln \beta_{ang}$ ),  $A$  is the area of the filled etch pit,  $a_{st}$  is the area corresponding to a solute unit, i.e.  $a_{st} = (a_{ang} \times b_{ang})/n$  (with  $n = 2$  being the number of  $\text{PbSO}_4$  molecules in an anglesite cell with dimensions  $a_{ang} \times b_{ang} \times c_{ang}/2$ ). From Eqn. (2) we obtain the following expression:

$$\gamma_{strain} = \frac{2kT \ln \beta_{ang}^{min}}{a_{ang} \times b_{ang}} \quad (3)$$

By using  $\beta_{ang}^{min} = 1.89 \pm 0.06$  in Eqn. (3), we obtain a specific total strain energy of  $11.4 \pm 0.6 \text{ mJ/m}^2$ . This value is similar to that obtained by Higgins and Hu [14] for the first monolayer formed on dolomite (104) surfaces. These authors conducted a series of AFM experiments to study the growth behaviour of the first two monolayers on dolomite surfaces and observed that, once the first monolayer was formed, the growth of a second monolayer was slow and subsequent layer-by-layer growth was highly inhibited even at high supersaturations.

According to Higgins and Hu [14], the total inhibition of continuous multilayer growth on dolomite was related to structural and/or compositional differences between the first monolayers and the dolomite (104) substrate. For the case of  $\text{PbSO}_4$  monolayers on a celestite (001) face, the situation is different and continuous multilayer growth occurs once the strain energy barrier was overcome by increasing the supersaturation. Furthermore, there was a strong dependency of the monolayer growth rates on the supersaturation and there were no significant differences in the growth kinetics of the first six monolayers (see Fig. 3). This seems to indicate a rapid reduction of the in-plane strain in the  $\text{PbSO}_4$  monolayers for growth at supersaturations above  $\beta_{ang}^{min}$ . However, the quality of the velocity data shown in Fig.3. does not allow us to quantify such a reduction.

In contrast, the development of anglesite spirals on the celestite (001) face only occurred for supersaturations higher than  $\beta_{ang}^{min}$ . Moreover, the shape of the spiral hillocks and step edges evolved as the first six monolayers were grown. These observations reveal a more complex strain field at the core of dislocations than that at the filled etch pits. Future research on the growth of anglesite hillocks as a function of supersaturation might provide interesting information on the influence of a local strain field on the kinetics of anglesite spiral growth on the celestite (001) face.



## 5. Conclusions

Our in situ AFM observations showed that anglesite monolayers can grow in structural continuity from pre-existing mono-steps on celestite (001). However, anglesite multilayer growth was inhibited for solution supersaturations with the values  $\beta_{ang} < 1.89 \pm 0.06$ . The inhibition of anglesite multilayer growth was a result of the generation of an inhomogeneous in-plane strain distribution. The minimum anglesite supersaturation required for continuous multilayer growth on the celestite (001) face allowed us to estimate the total strain energy in a single  $\text{PbSO}_4$  monolayer:  $11.4 \pm 0.6 \text{ mJ/m}^2$ . When the supersaturation was high enough to overcome the strain energy, continuous layer-by-layer and, occasionally, spiral growth of anglesite on celestite (001) faces was observed. The multilayer growth is in agreement with the Frank-van der Merwe epitaxial growth mechanism for high adhesion substrate-overgrowth pairs with low linear misfits. Furthermore, the results presented in this paper suggest that a  $\text{Pb}_x\text{Sr}_{1-x}\text{SO}_4$  solid solution with a wide range of compositions can grow at room temperature.

## Acknowledgments

This work was financially supported by the Universidad Complutense-Comunidad de Madrid (Project No. CCG08-UCM/AMB-3795 and Grant No. 910148-Superficies Minerales). The authors thank the Centro de Microscopia (UCM) for kindly providing them access to the AFM. The manuscript has been improved by the helpful comments of José M. Llorens and an anonymous reviewer.

## References

- [1] A.A. Chernov, *Modern Crystallography III* (Crystal Growth), Springer Verlag, 1984, p. 517
- [2] A. Pimpinelli, J. Villain, *Physics of Crystal Growth*, Cambridge University Press, Cambridge, 1998.
- [3] M. Prieto, P. Cubillas, A. Fernández-González, *Geochim. Cosmochim. Acta* 67 (2003) 3859.
- [4] C. Pérez-Garrido, L. Fernández-Díaz, C.M. Pina, M. Prieto, *Surf. Sci.* 601 (2007) L5499.
- [5] F. C. Frank, J. Van Der Merwe, *Proc. Roy. Soc. A*, 198 (1949) 216.
- [6] M. Volmer, A. Weber, *Z. Phys. Chem.* 119 (1926) 277
- [7] I.N. Stranski, V.L. Krastanov, *Akad. Wiss. Lit. Mainz Math.-Natur. Kl. Iib* 146 (1939) 797.
- [8] P. E. Hillner, A. J. Gratz, S. Manne, P. K. Hansma, *Geology* 20 (1992) 359.
- [9] C.M. Pina, U. Becker, P. Risthaus, D. Bosbach, A. Putnis, *Nature* 395 (1998) 483.
- [10] H.H. Teng, P.M. Dove, J.J. DeYoreo, *Geochim. Cosmochim. Acta* 64 (2000) 2255.
- [11] N. Sanchez-Pastor, C.M. Pina, J.M. Astilleros, L. Fernández-Díaz, A. Putnis, *Surf. Sci.* 581 (2005) L225.
- [12] A.G. Shtukenberg, J.M. Astilleros, A. Putnis, *Surf. Sci.* 590 (2005) L212.
- [13] K. Takahashi, M. Suzuki, M. Yoshimoto, H. Funakubo, *Japanese Journal of Applied Physics part 2-letters & express letters* 45 (2006) L138
- [14] S.R. Higgins, X. Hu, *Geochim. Cosmochim. Acta* 69 (2005) 2085.
- [15] J.M. Astilleros, C.M. Pina, L. Fernández-Díaz, A. Putnis, *Surf. Sci.* 545 (2003) L773.
- [16] J.M. Astilleros, C.M. Pina, L. Fernández-Díaz, A. Putnis, *Geochim. Cosmochim. Acta* 66 (2002) 3177.
- [17] J.M. Astilleros, C.M. Pina, L. Fernández-Díaz, A. Putnis, *Chem. Geol.* 193 (2003) 93.
- [18] D.L. Parkhurst, C.A.J. Appelo, *User's guide to PHREEQC (version 2). A computer program for speciation, batch-reaction, one-dimensional transport, and inverse geochemical calculations* (US Geological Survey. Water-Resources Investigations Report 99-4259, 2000) p. 312.
- [19] P. Risthaus, D. Bosbach, U. Becker, A. Putnis, *Physicochem. Eng. Aspects* 191 (2001) 201.
- [20] A.E. Murdaugh, M. Liddel, A.M. Schmidt, S. Manne, *Langmuir* 23 (2007) 5852.
- [21] J. Majzlan, A. Navrotsky, J. M. Neil, *Geochim. Cosmochim. Acta* 66 (2002) 1839.
- [22] M.A. Simonov, S.I. Troyanov, *Vestn. Mosk. Uni.* 4 (1987) 77.
- [23] C.M. Pina, A. Rico-García, *Macla* 9 (2008) 191 (in Spanish).